


An analytical model of diesel injector's needle valve eccentric motion

Chuqiao Wang^{1,2}, Moro Adams³, Tianyu Jin¹, Yu sun¹,
Andreas Roell^{1,4}, Fuqiang Luo¹  and Manolis Gavaises²

International J of Engine Research
1–13
© IMechE 2020
Article reuse guidelines:
sagepub.com/journals-permissions
DOI: 10.1177/1468087420987367
journals.sagepub.com/home/jer


Abstract

Past experimental studies have shown that the needle valve of high-pressure diesel injectors undergoes lateral movement and deformation, while the continuous increase in injection pressure enlarges the gap of the needle valve assembly. Two different analytical models, considering or omitting this change are presented here, linking the geometries of the needle valve assembly with the magnitude of needle valve tip lateral movement. It is found that the physical dimensions of the needle valve assembly and the injection pressure have a significant impact on the radial displacement of the needle. For example, for nominal clearances between the needle guidance and the needle valve of about 1–3 μm , the magnitude of the radial movement of the needle tip could reach tens of microns. The model that takes into account the variation of the gap between the needle guide and needle valve is found to give predictions closer to the experimental results.

Keywords

Diesel injector, needle valve assembly, fluid–structure interaction, eccentricity, cantilever beam, elastic deformation

Date received: 27 August 2020; accepted: 18 December 2020

Introduction

Despite that fact that research on development of “new energy vehicles” (NEVs) is on focus in an effort to decarbonize the transport sector, conventional fossil fuel internal combustion (IC) engines still supply around 25% of the energy in the world today.¹ For diesel engines equipped with a high-pressure common rail system, the fuel injector is one of the critical components for dispersing fuel into the combustion chamber. Control of in-cylinder emissions is achieved by multiple injection strategies, which require a prominent enhancement in needle dynamics within the injector. In this direction, both old and recent studies from the author's group and collaborators have demonstrated the impact of needle movement in high-pressure fuel injectors, which results in varying the flow characteristics within each nozzle hole and subsequently the atomization of the fuel at the outlets of the nozzle holes.^{2–8} Spray dynamics from various injector types affects the near nozzle atomization, penetration, cone angle, and air/fuel mixing in the combustion chamber, which are the key factors governing the quality of combustion and the pollutant formation.^{9–14} The movement of the needle valve within the injector is determined by the imbalance of forces acting on it. In the nominal design, the axis of the needle valve movement and the needle valve

body coincide, so the valve moves concentrically. Nonetheless, since the length of the needle valve guide is limited, the needle valve assembly is deformed due to installation and thermal stresses as well as hydraulic forces. These factors cause both an elastic deformation and an imbalance of forces in the radial direction that results in an eccentric movement of the needle valve.¹⁵

A variety of test equipment and research methods have been conducted to study the impact of the eccentric needle valve motion on internal flow characteristics and the spray patterns at the nozzle hole exits.^{16–19} One of the first methods used to detect needle eccentric moving within nozzles is the use of transparent nozzles. In Oda et al.²⁰ an experiment with a 10

¹School of Automotive and Traffic Engineering, Jiangsu University, Zhenjiang, China

²School of Mathematics, Computer Science & Engineering, City, University of London, London, UK

³Faculty of Mechanical Engineering, Accra Technical University, Accra, Ghana

⁴Institute of Energy Technology, OTH-Technical University of Applied Sciences, Amberg, Germany

Corresponding author:

Fuqiang Luo, School of Automotive and Traffic Engineering, Jiangsu University, Xuefu Road No. 301, Zhenjiang 210213, China.
Email: luofq@ujs.edu.cn

times large-scaled valve-covered-orifice (VCO) nozzle under eccentric needle movement was performed and the presence of complex flow regimes and atomization, especially at low needle lift, were observed. In Mitroglou et al.,^{21,22} the eccentric movement of the needle valve was visually observed in transparent real-size nozzles operating at pressures up to 60 MPa, while the compressibility effects inducing air flow back into the nozzle have been simulated in recent studies.²³ In Ohnishi et al.,²⁴ Gavaises et al.,²⁵ Gavaises,²⁶ Gavaises et al.,²⁷ Mitroglou et al.,²⁸ they studied the behavior of fuel spray in a multi-hole VCO nozzle experimentally and computationally. Specifically in²⁴ they found that the maximum eccentric needle radial displacements are 60 μm inside a VCO nozzle and 24 μm inside a micro-SAC nozzle. With the same methodology,²⁹ also measured eccentric needle displacement to be 0.04 mm. Another effective approach is to measure the transient needle motion using a high-speed X-ray phase-enhanced imaging (XPCI) technique.^{30,31} In Kastengren et al.,³² it was found that the maximum lift within the injectors was linearly related to the rail pressure, which is presumed to be related to the elastic deformation of the needle valve. They also measured the maximum and minimum eccentric radial displacement from four different injectors to be 0.065 and 0.016 mm, respectively. Similarly, in Zhang et al.,³³ X-ray phase XPCI was used to study the eccentricity of needle valve in diesel injectors with three different nozzle configurations. They showed in the studies that the radial vibration of the needle valve is mainly from -7 to $14 \mu\text{m}$, which is larger than the axial amplitude and increases with the number of orifices. Comprehensive experiments on the actual 3D movement of the needle within injectors were conducted using synchrotron radiation (SR) X-ray imaging technologies in Huang et al.,¹⁷ Torelli et al.,³⁴ Powell et al.³⁵ From their result, the boundary conditions needed to perform a numerical analysis on needle deformation could be obtained. For multi-hole nozzles, the needle lateral movement directly affects the distance between the needle location and inlet of each orifice, especially under cavitation conditions.¹⁶ Consequently, imparities in terms of mass flow rates, cavitation effects, and discharge coefficient at each hole exit lead to hole-to-hole variations. Once characterized, the upstream internal flow modeling is interfaced to the subsequent spray simulation, initializing the primary break-up model according to the transient flow parameters at each nozzle hole exit in terms of the vapor fraction, fuel velocity, and turbulence interaction.³⁶ Therefore, the presence of needle eccentricity causes flow variations in the nozzle, resulting in jet-to-jet spray asymmetries.^{5,7,19,37} XPCI has been also used to identify the detailed flow structures in nozzle replicas associated with the off-axis location of a needle valve relative to hole entrance, which gives rise to complex vortex (string) cavitation and cloud shedding.³⁸⁻⁴¹ However, the actual 3-D movement of the needle within injectors varies from injector to injector and

thus, shot-to-shot and injector-to-injector variations can be expected.

Needle valve assembly is one of the precision couplings in the high-pressure common rail system. The needle valve continuously undergoes relative axial movement in the inner cavity of the needle body. The valve guides in the nozzle ensure that the lateral needle valve motion is accurately controlled since the needle valve assembly is sensitive to clearance sliding. The upstream annular clearance between the needle valve guide and the injector body usually ranges from 1 to 3 μm .^{42,43} However, the experiment studies mentioned above have shown that the eccentricity of the downstream needle tip within different injectors ranges from a few to tens of μm , or in some cases even more than 100 μm . The reason for this order of magnitude difference still has not been reported. As injection pressures increase, the needle valve assembly experiences elastic deformation,⁴⁴⁻⁴⁶ expanding the clearance of the needle guidance,^{47,48} and deforming the moving components (control plunger, needle, and rod) in the axial direction.⁴⁹⁻⁵³ Nevertheless, to the best of authors' knowledge, there is no research conducted on the bending deformation of the needle in the radial direction and the relevance of the clearance gap changing in the upstream with the eccentricity of the needle tip. Real transient needle motion is an important boundary condition for numerical simulations; although many studies have been conducted on the internal flow characteristics and spray patterns with respect to needle eccentricity, the studies are either based on hypothetical magnitude^{36,54-57} or experimental data^{7,15,34,58} for specific injectors and few injection events.

The aim of the present work is to present a simplified model able to predict the lateral magnitude of the needle displacement among different geometries at various injection pressures, and thus to allow the injector design to be optimized. With regards to the research outputs reviewed above, a simplified model could be used to analyze the correlation between the needle guide gap and the lateral movement of the needle tip, based on the material and elastic mechanics. In order to simulate the rate of change of the clearance gap due to pressure difference accurately, a fluid-structure interaction approach was adopted. The influencing factors, such as geometric parameters, injection pressure, and variations in the clearance are quantified in sections "The impact of needle geometry (parametric studies)" and "The impact of fuel pressure", while the salient conclusions are summarized in the end.

Analytical model

As one of the precision pairs of the fuel supply system in high pressure common rail diesel engine, the tolerance clearance between the upstream needle guide and the needle body is between 1 and 3 μm . The aim is to maintain the performance of the seal and also restrain

the downstream needle movement in the lateral direction. However, the needle movement within the diesel injector follows a complex dynamics that includes rotation, wobbling, and deformation.

In order to better understand the influence of the needle geometry and fuel pressure on eccentricity and deformation, the following prerequisites and material mechanics were adopted in the relevant analytic model:

- (1) The impact of the force (such as fuel pressure and the spring force) on eccentricity of the needle is neglected; this implies that the forces and the bending deformation axes are on the same plane.
- (2) The needle valve assembly obeys the homogenization and continuity assumptions, signifying that the needle and the needle body density are evenly distributed across the entire occupied spaces without any voids. Also, the mechanical properties are the same at all points.
- (3) The needle valve assembly also obeys the isotropy assumptions, meaning that the elastomers have the same physical and mechanical properties in all directions.
- (4) The assumption of small deformation is introduced. That is, the deformation of the needle valve under the action of external forces is very small compared to its own geometric size, and thus the dimensional change caused by the deformation can be ignored.
- (5) Based on the above-mentioned assumptions, the impact of the torsion and shear on the needle movement is minimal as compared to the bending deformation, and thus could also be ignored. It should be mentioned here that although the moving components in the injector are undergoing extension or compression along the z-axis, the maximum deformation is located at the upper end of the control plunger, which is far away from the needle tip.^{49,50} Besides, as a thin rod, the difference in dimension with regards to the length and width is large, hence the influence of the expansion and shrinking on the lateral deformation is also neglected.
- (6) The lateral motion of the needle is assumed to be planar,³⁰ implying that the needle is moving to one direction; thus, the transverse of the movement has not been considered in this model.

Accordingly, the lateral deformation of the needle is simplified to symmetric bending deformation, which could be solved by the superposition method. When the magnitude of bending deformation is small and the material complies with Hooke's law, the differential equation of deflection curve is linear. The relationship between each load and bending moment is linear and the corresponding bending deformation caused could be superimposed.⁵⁹

Considering the needle as a cantilever beam, then the needle guide part could be considered as a fixed bearing, because the gap of the upstream needle guide and needle body is minimal.^{15,30} When the needle experiences eccentricity, the pressure fuel on the needle tip not only forces the needle to move in the longitudinal dimension, but it also bends it in the lateral dimension. Given the approximate differential equation of the deflection curve⁵⁹:

$$\frac{d^2 \omega_B}{dx^2} = \frac{M}{EI} \quad (1)$$

The bending deformation can be calculated by:

$$\omega_B = -\frac{Ml^2}{2EI} \quad (2)$$

where ω_B represents the deflection, M represents the bending moment caused by the fuel pressure, E represents the elastic modulus of the needle, while I represents the inertia moment.

As shown in the Figure 1, there are four different positions regarding the needle movement: (i) vertical movement without any eccentricity and distortion; (ii) undeformed needle with eccentricity; (iii) eccentricity with further deformation; and (iv) further deformation taking the change in clearance into consideration.

Table 1 illustrates the corresponding parameters shown in Figure 1. The clearance of the needle guide and needle (e_1) is between 1 and 3 μm . This clearance is used to restrain the lateral movement of the needle. However, because of this gap, eccentric movement of the needle is realized during operation. When the needle experiences only eccentric movement, the correlation of the downstream eccentricity magnitude e_2 and the upstream gap value e_1 can be obtained from the geometric relationship between the components of the needle valve assembly:

$$\frac{e_1}{e_2} = \frac{l_2}{l_1} \quad (3)$$

$$e_2 = \frac{l_1 \cdot e_1}{l_2} \quad (4)$$

Furthermore, due to the high pressure acting on the needle tip, the needle will continue deforming after its contact with the nozzle body. The bending moment caused by fuel pressure could be calculated as:

$$M = F \cdot l = P \cdot S \cdot (e_2 + e_3) \cdot \cos\alpha \quad (5)$$

$$S = \frac{\pi \cdot d_1^2}{4} \quad (6)$$

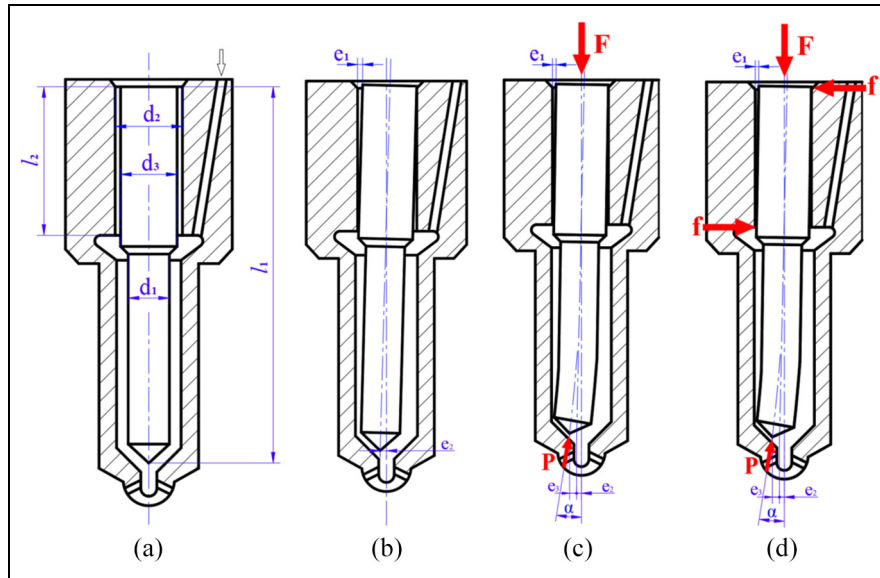


Figure 1. Schematic diagram of needle eccentricity and further deformation: (a) vertical needle, (b) eccentricity, (c) deformation, and (d) deformation (based on the guidance deformation).

Table 1. Relevant parameters.

Names of the parameters	Meanings of the parameters
d_1	The diameter of the downstream needle
d_2	The diameter of the needle guidance (on the needle body)
d_3	The diameter of the upstream needle
l_1	The length of the needle
l_2	The length of the needle guidance
e_1	The gap between the upstream needle and the needle guidance
e_2	The eccentric magnitude of the needle tip (non-deformation)
e_3	Further deformed magnitude of the needle tip caused by the fuel pressure
A	Dip angle between the axis of the needle and needle body (after eccentricity and deformation)
F	Resultant force of the spring force and control plunger applied force
P	Fuel pressure acts on the needle tip
f	Stress acts on the inlet and outlet of the clearance

where S represents the projected area of the needle tip due to equation (1); then

$$e_3 = \frac{Ml^2}{2EI} = \frac{M(l_1 - l_2)^2}{2EI} \tag{7}$$

where I is the inertial moment, which for circular cross section is:

$$I = \frac{\pi d_1^4}{64} \tag{8}$$

It should be noted here that there is a reacting force located at the inlet and outlet of the gap between the needle and the needle body because of the limitation of the needle movement in the lateral direction. Nevertheless, due to the Saint Venant's Principle,⁶⁰ the effect of this stress and consequent bending moment on the far-away needle tip could be neglected.

By inserting equations (6), (7), and (8) into equation (5), the final equation of the deformation magnitude is:

$$e_3 = \frac{e_2}{Ed_1^2/8P \cdot \cos\alpha \cdot (l_1 - l_2)^2 - 1} \tag{9}$$

Since the magnitude of the needle eccentricity with deformation caused by elastic bending (in micron level) is much smaller than that of the geometric size of the needle assembly (in millimeter level), the angle between the axis of the needle and needle movement is so small that, it could be considered to be zero. Consequently, to simplify the model, the final magnitude equation will be:

$$e_3 = \frac{e_2}{Ed_1^2/8P \cdot (l_1 - l_2)^2 - 1} \tag{10}$$

Then the total lateral displacement taking both the eccentricity and deformation into account is:

Table 2. Relevant parameters.

Names of the parameters	Meanings of the parameters	Value
d_1	The diameter of the downstream needle	3.2 mm
d_2	The diameter of the needle guidance	3.8015 mm
d_3	The diameter of the upstream needle	3.8 mm
e_1	Fit clearance of the needle guidance	2 μm
l_1	The length of the needle	41.9 mm
l_2	The length of the needle guidance	12.8 mm
m	Mass of the needle	3.3 g

$$e = e_2 + e_3 \quad (11)$$

The impact of needle geometry (parametric studies)

The analytical model illustrated above was used to investigate the influence of the needle geometric parameters on the magnitude of the eccentricity. A typical needle valve assembly produced by WFIERI, China^{61,62} was adopted to do the study; the values of relative parameters are given in Table 2.

In order to investigate how the clearance upstream of the needle valve affects the magnitude of the eccentricity at its tip, the value of e_1 was set as 1, 1.5, 2, 2.5, and 3 μm , respectively.

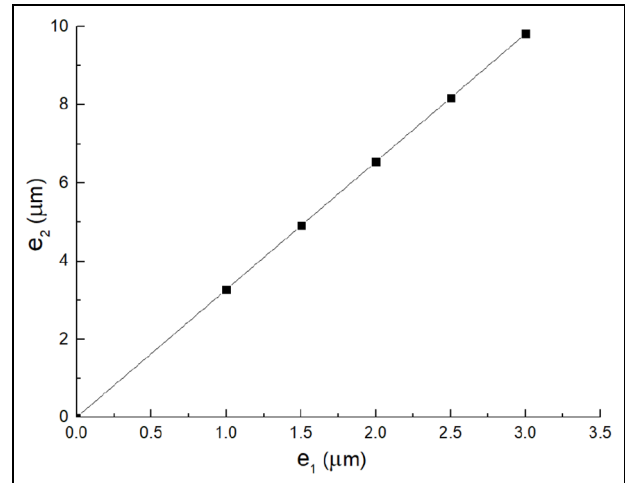
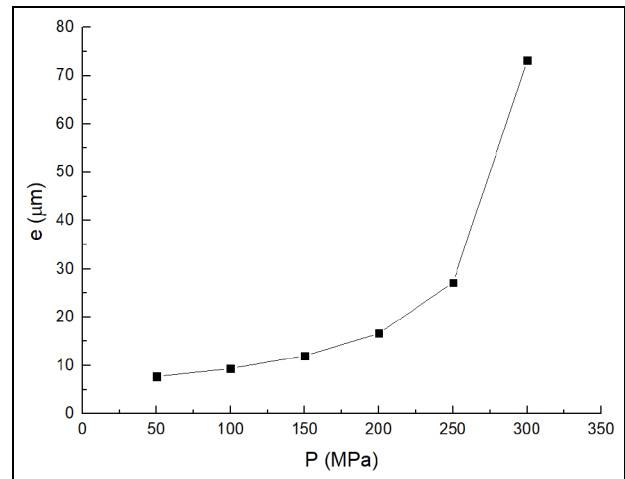
As shown in Figure 2, when the needle is not deformed, the relationship between e_1 and e_2 is linear. Besides, the tip eccentric magnitude is inversely proportional with the annular clearance of the needle guide and proportional to the needle length.

The impact of fuel pressure

Without considering the change of the annular gap of the needle guide

When the needle undergoes eccentricity with deformation, the relevance between the fuel pressure and the lateral displacement of the tip can be calculated with equations (10) and (11). As shown in Figure 3, the relevant values of the parameters used are indicated in Tables 2 and 3.

When the pressure is lower than 200 MPa, the correlation between the fuel pressure and the total lateral displacement demonstrates a linear change. Furthermore, the lateral displacement only changes around 7 μm for pressures below 200 MPa. However, when the fuel pressure is larger than 200 MPa, the total eccentric magnitude increases noteworthy with fuel pressure, reaching 55 μm for 300 MPa. It can be seen from equation (10) that the further bending magnitude e_3 is based on the

**Figure 2.** Correlation of e_1 and e_2 .**Figure 3.** Correlation of lateral displacement (e) with pressure.

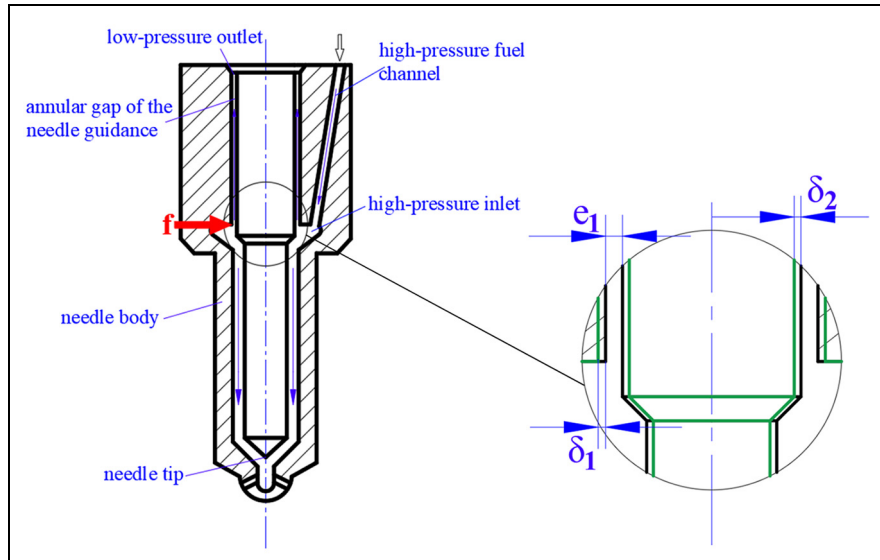
eccentricity e_2 , reflected in the “-1” of the denominator. This influence is nearly linear under 200 MPa but changed significantly beyond 200 MPa, which could be the reason why the total deformation e varies prominently when the pressure is larger than 200 MPa.

Considering the variation in the annular gap of the upstream needle guidance

Theoretical calculation. As the injection pressure of the fuel supply system increases, the high-pressure fuel filling the delivery chamber and the fit clearance between the needle guide and needle body place a large load on the needle valve assembly. This load will distort the needle valve couplings and thus, will increase the radial clearance between the needle guidance and the needle body. Some studies^{47,48} have shown that this gap will be doubled or even tripled compared to its original size. Moreover, unstable fuel flow within the injector occurs

Table 3. Material characteristics of needle valve couples.

Name	Materials	Elastic modulus (GPa)	Poisson ratio	Density (kg/m ³)
Needle	W18Cr4V	218	0.3	7830
Needle body	18Cr2Ni4WA	206	0.3	7890

**Figure 4.** Schematic of the needle valve assembly, green lines illustrates the wireframe after the deformation.

easily as the clearance expands, increasing the possibility of the radial eccentric movement of the needle valve. According to the widely used annular gap flow theory and linear elastic theory^{63,64} in the industry for analyzing the lubrication and leakage, the radial displacement caused by the expansion of the needle body could be expressed as:

$$\delta_1 = P_x \frac{d_2}{2E_1} \left(\frac{d_2 - d_3}{d_2 + d_3} + \lambda_1 \right) \quad (12)$$

The radial displacement caused by the compression of the needle valve could be indicated as:

$$\delta_2 = P_x \frac{d_3}{2E_2} - P_1 \frac{d_3}{2E_2} \lambda_2 \quad (13)$$

Where P_x represents the fuel pressure located at the x position along the axis of the needle valve assembly; P_1 represents the fuel pressure in the delivery chamber; d_2 and d_3 are the diameters of the needle guidance and the upstream needle, respectively; E_1 and E_2 are the elastic modulus of the needle body and needle valve respectively; λ_1 and λ_2 are the Poisson ratio of the needle body and needle valve respectively.

So the total radial displacement of the clearance is:

$$\delta = \delta_1 + \delta_2 \quad (14)$$

Figure 4 illustrates different components of the needle valve assembly and the variation in the annular gap between the needle and the needle guidance. The black and green outlines shown in the zoomed view at the high-pressure inlet represent the model and after the deformation, respectively. As shown in Figure 4, the high-pressure inlet is found at the lower end of the needle guide close to the delivery chamber, while the low-pressure outlet is located at the upper end surface of the valve. Since the radial force F loaded at the high-pressure inlet is a function of rail pressure,⁴⁸ the change in the clearance of the lower end would be higher than that of the upper end. In order to investigate the maximum lateral deformation, the deformation at the upper surface end is neglected. It should be noted here that equations (12) and (13) are not totally precise because both of them are derived by simplifying the stress condition loaded on the needle valve assembly into a 2D plane configuration. Since the fuel pressure distributed around the surface of the needle and needle body in the axial direction is very complex (and hard to obtain due to the complicated flow configuration), the equations (12) and (13) can serve only as approximations^{43,64} or the 3D problem. Based on this simplification, the P_x is equal to the P_1 in equations (12) to (14); then the total displacement could be expressed as:

$$\delta = P_1 \frac{d_2}{2E_1} \left(\frac{d_2 - d_3}{d_2 + d_3} + \lambda_1 \right) + P_1 \frac{d_3}{2E_2} (1 - \lambda_2) \quad (15)$$

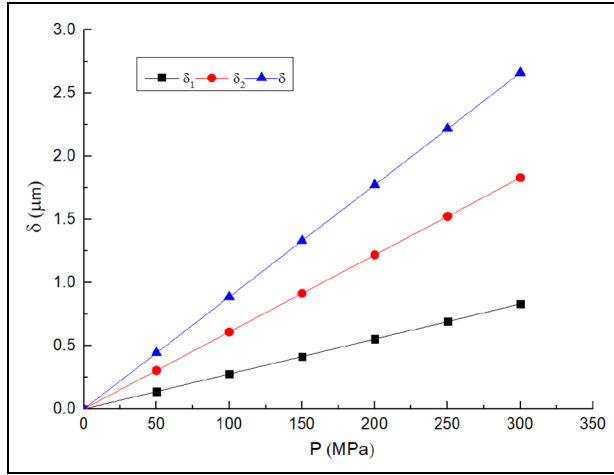


Figure 5. Correlation of the radial change in the gap with pressure.

Moreover, it is assumed that there is no pressure loss in the fuel supply system, so the injection pressure P is equal to the fuel pressure in the delivery chamber P_1 . Given the detailed parameters shown in the Tables 2 and 3, the results are shown in Figure 5.

It should be noted here the results obtained from Figure 5 are based on equations (12) to (15), which are the same with equations in reference⁶⁴ used to build an analytical model for the leakage at the piston/cylinder interface. In their study, they verified their model by comparing the simulated and experimentally measured piston/cylinder interface leakage rates on a high-pressure pump CB18 at different pressures up to 160 MPa. In other words, equations (12) to (15) have been already validated in reference,⁶⁴ implying the results in Figure 5 could be adopted.

As shown in Figure 5, the total radial deformation of the gap increases linearly with injection pressure, reaching $2.66 \mu\text{m}$ at 300 MPa. Besides, the needle is deformed more in the radial direction than the needle body. Therefore, when taking the change in the clearance of the needle guidance into consideration, the final lateral displacements could be expressed as follows:

$$e_1' = e_1 + \delta \quad (16)$$

$$e_2' = \frac{l_1 \cdot e_1'}{l_2} \quad (17)$$

$$e_3' = \frac{e_2'}{Ed_1^2/8P \cdot (l_1 - l_2)^2 - 1} \quad (18)$$

$$e' = e_2' + e_3' \quad (19)$$

As shown in Figure 6, although the tendency of the total radial eccentric magnitude is similar to that shown in Figure 3, the curve is steeper because the gap

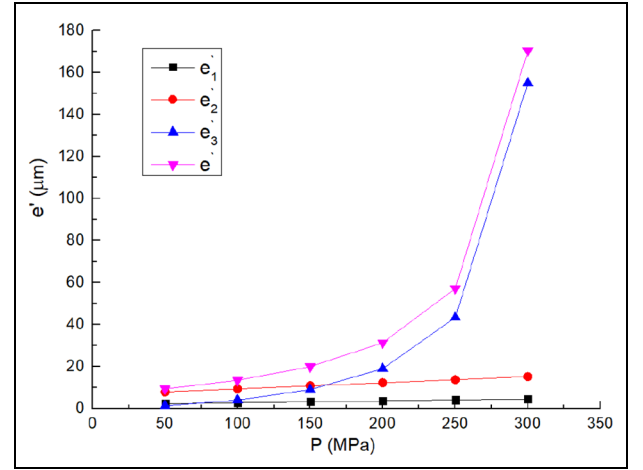


Figure 6. Correlation of lateral displacement with pressure considering the gap variations.

variations has been taken into consideration. Generally, one of the features of the needle lateral movement is that the oscillation amplitude increases with increasing injection pressure.¹⁷ The lateral displacement obtained from theoretical calculation in this section is around $14 \mu\text{m}$ at 100 MPa and $20 \mu\text{m}$ at 150 MPa. Several studies have been conducted to measure the lateral moving magnitude, ranging from $15 \mu\text{m}$ at 100 MPa for different injector geometries^{34,35} to $18\text{--}25 \mu\text{m}$ at 160 MPa for a three holes diesel injector.¹⁷ Therefore, it can be concluded that the theoretical and experimental results are closer compared to those of Figure 3. However, because of the limitation of conducting experiments for pressures up to 300 MPa, to the best of author's knowledge, there is no prior publication reporting measurements of the lateral displacement of the needle valve. In addition, it should be noted that the eccentric movement of the needle valve depends on the nozzle geometry and hydraulic behavior of fuel flow within the nozzle, giving rise to the uncertainty of predicting its actual movement within the diesel injector.

Fluid–structure interaction approach. Case setup. The empirical equations could give some information on the gap change, but it is fair to say that this is only an approximation due to the complex flow conditions within the diesel injector. An alternative approach used to estimate the needle deformation is to utilize fluid–structure interaction simulations under real working conditions; ANSYS Workbench was used in the present study. In order to reduce the computational cost, a half model was adopted due to the axis-symmetric structure of the needle valve assembly. Also, the downstream of the needle valve assembly was omitted due to the Saint Venant's Principle.

Figure 7 is the diagram of needle valve assembly model. As shown in the Figure 7(a), the computational mesh utilized for the fluid structure interaction simulations is divided into two parts: the solid domain consists

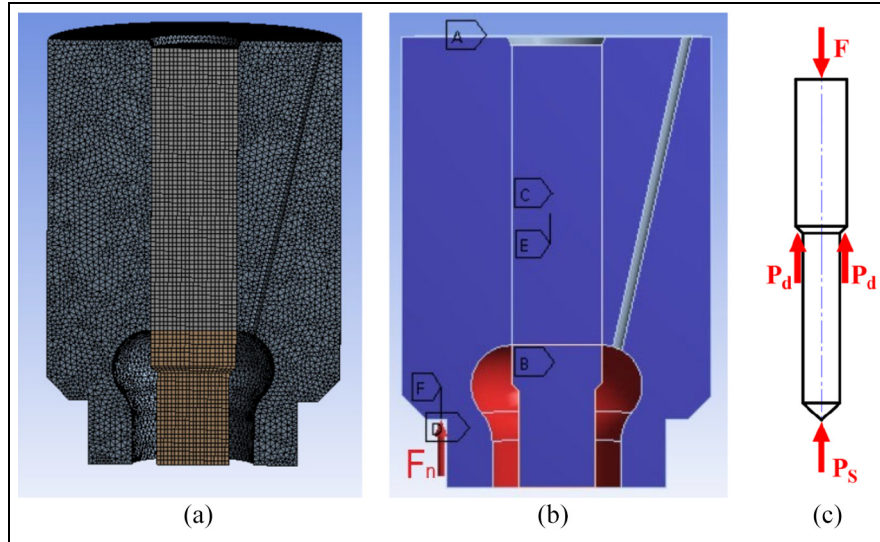


Figure 7. Needle valve assembly model: (a) solid domain of computational grids, (b) boundary conditions and constraints, and (c) loads of the needle.

of the needle valve and needle body. The fluid domain is the fuel filling the gap between these two solid parts. The nodes of the solid and fluid domains are kept one-to-one correspondence with each other. The contact surface with the fuel filling the gap is densified to simulate the deformation caused by the high fuel pressure. The fuel flow through the gap is regarded as laminar flow due to the marginal gap and lower fluid speed,⁴³ and the mesh of the gap film is divided into five layers. The final count of cells for the solid and fluid domain are 900,000 and 600,000, respectively.

Figure 7(b) presents the boundary conditions and constraints for the structural simulation. Since the needle valve assembly model has been symmetrically processed, symmetry constraints are imposed to the cut-plane of the needle and the needle body. The top surface of the needle was fixed, while the bottom surface was set as constrain free. Since the needle body is fixed to the injector by the clamping nut on the valve body shoulder, the contact surface between the needle body and injector was set as support face. The fuel pressure was imported on the delivery chamber and pressure bearing surface of the needle, so the fuel contact surfaces between the fluid (fuel) and the solid (internal face and external surface of the needle and needle body) are set as coupling surfaces.

F_n in Figure 7(b) represents the applied stress acting on the shoulder of the needle body caused by the tightening torque of the clamping nut. Given an estimated torque⁴⁸ of $80 \text{ N}\cdot\text{m}$ and area of the shoulder as 64.75 mm^2 , the stress F_n is 535.13 MPa . Figure 7(c) illustrates the loading on the needle valve. The needle is exposed to three areas where the forces are acting during movement. F acts on the upper end and represents the resultant force of the spring force and control plunger force, P_d and P_s represent the fuel pressure in the

delivery chamber and nozzle's sac volume, respectively; then:

$$F - P_d \frac{\pi \cdot (d_3^2 - d_1^2)}{4} - P_s \frac{\pi \cdot d_1^2}{4} = ma \quad (20)$$

It should be noted here that, viscous shear force by the fluid in the annular gap between the needle and needle body could be neglected because the clearance is very small.^{43,48} Assuming that the fuel pressure in the delivery chamber and sac volume are the same, then:

$$F - P_d \frac{\pi \cdot d_3^2}{4} = ma \quad (21)$$

$$P_F = \frac{4F}{\pi \cdot d_3^2} \quad (22)$$

where a is the acceleration of the needle valve. As known, the speed of the needle valve during the opening and closing phases can reach $\sim 3 \text{ m/s}$, and the time of the closing process for the needle from the maximum needle lift is approximately $\sim 0.25 \text{ ms}$.⁴⁷ Taking the fuel pressure of 200 MPa as an example, the F and P_F are calculated to be 2267 N and 200 MPa respectively.

The boundary conditions of the inlet and outlet for the fluid domain were set as pressure boundary conditions. The inlet pressure was set as $50, 100, 150, 200, 250,$ and 300 MPa respectively, while the outlet pressure was 0.1 MPa . A pressure-based segregated PISO algorithm was used to couple the velocity and pressure fields, along with the discretization in both space and time of second-order scheme. Physical properties of fluid and solid domain are shown in the Tables 3 and 4.

Table 4. Thermodynamic properties.

Fuel properties	Value
Density (kg/m^3)	836.61
Dynamic viscosity ($\text{mPa} \cdot \text{s}$)	3.94

Results and discussion. Two different operating conditions have been simulated. In the first case, the needle was assumed to move at a speed of 3 m/s and in the second, the needle was maintained at a given lift.

Figure 8 presents the contour of lateral deformation, that is, in the x -axis direction for the two cases examined. Four probes were set to detect the deformation value of the needle valve as well as needle body, where A was defined as the deformation at the left side and B was defined as the deformation at the right side (with the high pressure fuel passage). Both cases show the same trend with slight differences. The change in the gap is larger at the inlet, since the high pressure inlet is close to the delivery chamber while the low pressure outlet is on the upper end.

The variations of the clearance at probe A and B under both working conditions are listed in Table 5; the

total deformation of both A and B increases linearly with the rise of the fuel pressure while the total deformation in the lateral direction of B is larger than that of A. This is because of the high pressure fuel in the duct on the right-hand-side of the needle valve body, that causes the formation of a cavity and, therefore, causing higher deformation. Besides, when the needle valve moves at a speed of 3 m/s, the total lateral deformation of both A and B is slightly smaller than that calculated under the fixed needle lift case.

As shown in the Figures 8 and 9, the changing of the clearance and the lateral displacement, as predicted by fluid–structure interaction simulation, is larger than that estimated by the empirical equations. Figure 9(a) shows the results obtained at 3 m/s; the lateral motion amplitude is $15.1822 \mu\text{m}$ at 100 MPa and $24.1125 \mu\text{m}$ at 150 MPa. Figure 9(b) presents the results when needle lift is fixed; the lateral magnitude is $15.1994 \mu\text{m}$ at 100 MPa and $24.2139 \mu\text{m}$ at 150 MPa. The relative error of deformation between the two working conditions varies from 2.18% to 59.95% over the pressure range of 50 to 300 MPa. Besides, the eccentricity magnitude at 100 MPa mentioned in section “Theoretical calculation”³⁴ also shows the average radial motion fluctuating within $27 \mu\text{m}$ at 150 MPa. The FSI

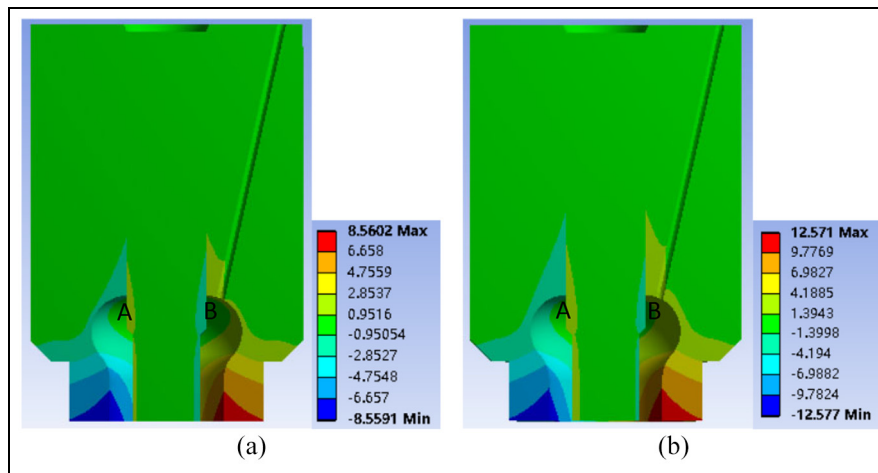


Figure 8. Deformation contour in the lateral direction at 200 MPa fuel pressure (μm): (a) deformation when needle moving at 3 m/s and (b) deformation when needle still.

Table 5. Variations of clearance (μm).

Pressure (MPa)	3 m/s		0 m/s	
	Total deformation at A	Total deformation at B	Total deformation at A	Total deformation at B
0	0	0	0	0
50	0.32209	0.380868	0.322888	0.381668
100	1.08977	1.23053	1.09346	1.23419
150	1.914241	2.01303	1.93113	2.02991
200	2.6705	2.8903	2.6739	2.8938
250	3.4837	3.6806	3.4847	3.6999
300	4.3149	4.4664	4.3382	4.4896

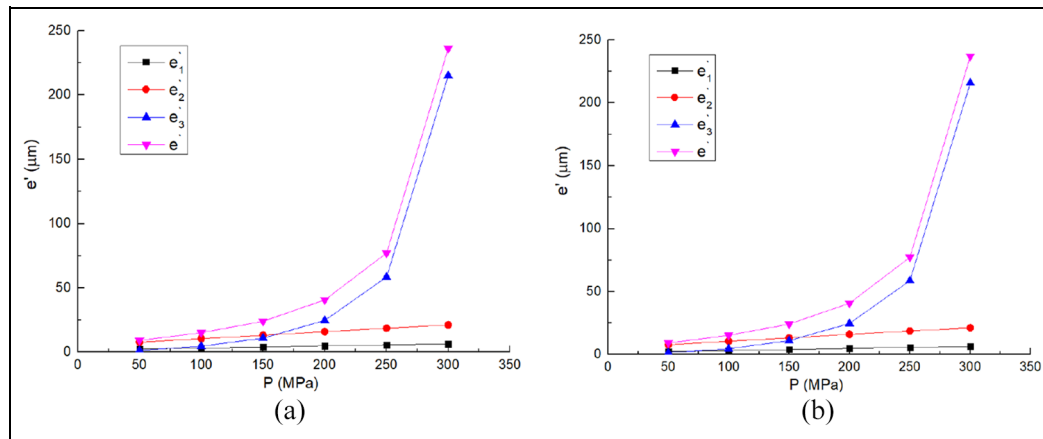


Figure 9. Correlation of lateral displacement with pressure by FSI: (a) correlation when needle moving at 3 m/s and (b) correlation when needle is fixed.

approach takes into consideration the distribution of fuel pressure around the surface of the needle valve, which is ignored in the theoretical calculation. Comparing the lateral movement magnitude at 100 and 150 MPa, as obtained by both the theoretical calculation and the FSI approach, against the aforementioned experimental data, it can be concluded that the results of FSI approach is closer to the experiments. However, it should be mentioned here that since the geometry of the needle is not the same among different injectors, and the needle movement in actual injectors is subjected to random motion, the lateral displacements could vary a lot from injector to injector, or even during each successive needle valve opening within the same injector.³⁰ Besides, the fluctuations of the injection pressure and oscillations of the fuel pressure in the delivery chamber and the nozzle's sac volume are also contributing to the lateral displacement, which varies among injectors as well.

Conclusion

An analytical model that is able to compute the magnitude of the lateral displacement of the needle valve was presented in this study. Elastic material mechanics and fluid structure interactions were used to analyze the possible factors affecting needle eccentricity as well as bending deformation. The study shows good similarity with the experimental value, implying the possibility of optimization for the design of the injector. The detailed conclusions are presented as followings:

- (1) When the gap of the needle valve and needle guide is fixed, the eccentricity of the needle tip changes linearly with the ratio of the needle length to the needle guide length. Therefore, increasing the needle guide length or reducing the needle length

could effectively suppress the downstream eccentricity of the needle tip.

- (2) When the fuel pressure is below 100 MPa, the eccentricity is also small and changes almost linearly but minimal with the fuel pressure. Nevertheless, as the fuel pressure increases to 100 MPa, especially more than 200 MPa, the total eccentricity increases remarkably, and the changes rate of the eccentricity increases with the growth of fuel pressure.
- (3) Due to higher fuel injection pressure, the needle valve will inevitably deform. This deformation will enlarge the clearance in the needle valve guidance, leading to the increment of the total radial displacement of the needle.
- (4) When considering the deformation of the needle valve assembly, the total lateral displacement of the needle tip is more in line with the test results of other relevant scholars. So in practical terms, the variation of the clearance in the needle guidance should not be neglected.


Declaration of conflicting interests

The author(s) declared no potential conflicts of interest with respect to the research, authorship, and/or publication of this article.

Funding

The author(s) disclosed receipt of the following financial support for the research, authorship, and/or publication of this article: This work was supported by the National Natural Science Foundation of China (No. 51476072), and the China Scholarship Council (CSC No. 201808320261).

ORCID iD

Fuqiang Luo  <https://orcid.org/0000-0002-1009-1837>

Reference

1. Reitz RD, Ogawa H, Payri R, et al. IJER editorial: the future of the internal combustion engine. *Int J Engine Res* 2020; 21(1): 3–10.
2. Gavaises M. Modeling of diesel fuel injection processes. PhD Thesis, Imperial College, University of London, 1997.
3. Koukouvinis P, Vidal-Roncero A, Rodriguez C, Gavaises M and Pickett L. High pressure/high temperature multiphase simulations of dodecane injection to nitrogen: application on ECN Spray-A. *Fuel* 2020; 275: 117871.
4. Cristofaro M, Edelbauer W, Koukouvinis P and Gavaises M. A numerical study on the effect of cavitation erosion in a diesel injector. *Appl Math Model* 2020; 78: 200–216.
5. Gavaises M, Mithun MG, Koukouvinis P, Gold M and Pearson R. Numerical simulation of fuel dribbling and nozzle wall wetting. *Int J Engine Res* 2021.
6. Mithun MG, Koukouvinis P and Gavaises M. Numerical simulation of cavitation and atomization using a fully compressible three-phase model. *Phys Rev Fluids* 2018; 3(6): 0–3.
7. Gold M, Pearson R, Turner J, Sykes D, Stetsyuk V, Sercey G, Crua C, Koukouvinis P and Gavaises M. Simulation and measurement of transient fluid phenomena within diesel injection. SAE technical paper 2019-01-0066, 2019.
8. Agarwal A and Trujillo MF. The effect of nozzle internal flow on spray atomization. *Int J Engine Res* 2020; 21: 55–72.
9. Wang B, Li T, Ge L and Ogawa H. Optimization of combustion chamber geometry for natural gas engines with diesel micro-pilot-induced ignition. *Energy Convers Manag* 2016; 122: 552–563.
10. Li T and Ogawa H. Analysis of the trade-off between soot and nitrogen oxides in diesel-like combustion by chemical kinetic calculation. *SAE Int J Engines* 2012; 5(2): 94–101.
11. Shibata G, Nishiuchi S, Xie P, Takai S, Ogawa H and Kobashi Y. Measurements of fuel adhesion on cylinder walls and fuel wall-flow behavior with post diesel fuel injections. *Int J Engine Res* 2020; 21(2): 352–366.
12. Fansler TD, Trujillo MF and Curtis EW. Spray-wall interactions in direct-injection engines: An introductory overview. *Int J Engine Res* 2020; 21: 241–247.
13. Payri R, De La Morena J, Monsalve-Serrano J, Pesce FC and Vassallo A. Impact of counter-bore nozzle on the combustion process and exhaust emissions for light-duty diesel engine application. *Int J Engine Res* 2019; 20: 46–57.
- [14] Gavaises M and Arcoumanis C. Modelling of sprays from high-pressure swirl atomizers. *Int J Engine Res* 2001; 2: 95–117.
- [15] Battistoni M, Xue Q, Som S and Pomraning E. Effect of off-axis needle motion on internal nozzle and near exit flow in a multi-hole diesel injector. SAE technical paper 2014-01-1426, 2014.
- [16] Chiatti G, Chiavola O, Frezzolini P and Palmieri F. On the link between diesel spray asymmetry and off-axis needle displacement. *Appl Sci* 2017; 7(4): 375.
17. Huang W, Moon S, Gao Y, Li Z and Wang J. Eccentric needle motion effect on near-nozzle dynamics of diesel spray. *Fuel* 2017; 206: 409–419.
18. Wang C, Moro A, Xue F, Wu X and Luo F. The influence of eccentric needle movement on internal flow and injection characteristics of a multi-hole diesel nozzle. *Int J Heat Mass Transf* 2018; 117: 818–834.
19. Moro A, Luo T, Wang C and Luo F. Eccentric needle displacement effect on spray formation from a multi orifice diesel injector. *Heat Mass Transf* 2019; 55: 2623–2635.
20. Oda T, Hiratsuka M, Goda Y, Kanaike K and Ohsawa K. Experimental and numerical investigation about internal cavitating flow and primary atomization of a large-scaled vco diesel injector with eccentric needle. In: *Proceeding of the ILASS-Europe 2010, 23rd Annual Conference on Liquid Atomization and Spray Systems*, Brno, Czech Republic, 6–8 September 2010, pp. 1–7.
21. Mitroglou N, McLorn M, Gavaises M, Soteriou C and Winterbourne M. Instantaneous and ensemble average cavitation structures in Diesel micro-channel flow orifices. *Fuel* 2014; 116: 736–742.
22. Mitroglou N, Gavaises M, Nouri JM and Arcoumanis C. Cavitation inside enlarged and Real-size fully transparent injector nozzles and its effect on near nozzle spray formation. In: *Proceeding of the DIPSI Work, 2011 Droplet Impact Phenomena and Spray Investigation*, Bergamo, Italy, 27 May 2011, pp. 33–45.
23. Santos E, Shi J, Gavaises M, Soteriou C and Winterbourn M. Investigation of cavitation and air entrainment during pilot injection in real-size multi-hole diesel nozzles. *Fuel* 2020; 263: 116746.
24. Ohnishi H, Yoshida T and Arifuku T. Characteristics fuel discharge in multihole VCO. *Trans Japan Soc Mech Eng B* 1995; 61(9): 1554–1560.
25. Gavaises M, Arcoumanis C, Roth H, Choi Y.S and Theodorakakos A. Nozzle flow and spray development from VCO diesel injector nozzles. In: *Proceedings of THIESEL 2002 Conference on Thermo- and Fluid-Dynamic Processes in Diesel Engines*, Valencia, Spain, 11–15 September, 2002.
26. Gavaises M. Flow in valve covered orifice nozzles with cylindrical and tapered holes and link to cavitation erosion and engine exhaust emissions. *Int J Engine Res* 2008; 9: 435–447.
27. Gavaises M, Papoulias D, Giannadakis E, Andriotis A, Mitroglou M and Theodorakakos A. Comparison of cavitation formation and development in diesel VCO nozzles with cylindrical and converging tapered holes. In: *Proceedings of THIESEL 2008 Conference on Thermo- and Fluid-Dynamic Processes in Diesel Engines*, Valencia, Spain, 8–10 September, 2008.
28. Mitroglou N, Gavaises M and Arcoumanis C. Spray stability from VCO and a new diesel nozzle design concept. In: *Proceedings of IMechE Conference of Fuel Injection Systems for IC Engines*, London, UK, 14–15 March, 2012.
29. Shoji T. Effect of cycle-to-cycle variations in spray characteristics on hydrocarbon emission in DI diesel engines (Visualization of sac inner flow, needle valve motion and cycle-to-cycle variations in diesel spray). *JSME Int Journal Ser B Fluids Therm Eng* 1997; 40(2): 312–319.

30. Kastengren AL, Tilocco FZ, Powell CF, Manin J, Pickett LM, Payri R and Bazyn T. Engine combustion network (ECN): measurements of nozzle geometry and hydraulic behavior. *At. Sprays* 2012; 22(12): 1011–1052.
31. Wu Z, Zhao W, Li Z, Deng J, Hu Z and Li L. A review of engine fuel injection studies using synchrotron radiation x-ray imaging. *Automot Innov* 2019; 2(2): 79–92.
32. Kastengren AL, Powell CF, Liu Z, Fezzaa K and Wang J. High-speed x-ray imaging of diesel injector needle motion. In *Proceedings of the ASME Internal Combustion Engine Division 2009 Spring Technical Conference (ICES2009)*, Milwaukee, Wisconsin, USA, 3-6 May 2009, pp. 1–12.
33. Zhang X, Liu J and Wang J. Effect of fuel and nozzle geometry on the off-axis oscillation of needle in diesel injectors using high-speed X-ray phase contrast imaging. *J Instrum* 2016; 11(05): 1–13.
34. Torelli R, Matusik KE, Nelli KC, Kastengren AL, Fezzaa K, Powell CF and Som S. Evaluation of shot-to-shot in-nozzle flow variations in a heavy-duty diesel injector using real nozzle geometry. SAE technical paper 2018-01-0303, 2018.
35. Powell CF, Kastengren AL, Liu Z and Fezzaa K. The effects of diesel injector needle motion on spray structure. *J Eng Gas Turbines Power* 2011; 133(1): 012802.
36. Chiatti G, Chiavola O, Palazzoni M and Palmieri F. Diesel spray modeling under off-axis needle displacement. SAE Technical Paper 2015-01-0922, 2015.
37. Risi AD, Colangelo G and Laforgia D. An experimental study of high pressure nozzles in consideration of hole-to-hole spray abnormalities. SAE Technical Paper 2000-01-1250, 2000.
38. Karathanassis IK, Trickett K, Koukouvinis P, Wang J, Barbour R and Gavaises M. Illustrating the effect of viscoelastic additives on cavitation and turbulence with X-ray imaging. *Sci Rep* 2018; 8(1): 1–15.
39. Karathanassis IK, Koukouvinis P, Efstathios K, Lee ZL, Wang J, Mitroglou N and Gavaises M. High-speed visualization of vortical cavitation using synchrotron radiation. *J Fluid Mech* 2018; 838: 148–164.
40. Karathanassis IK, Koukouvinis P and Gavaises M. Multiphase phenomena in diesel fuel injection systems. In *Simulations and Optical Diagnostics for Internal Combustion Engines: Current Status and Way Forward*, Singapore: Springer Singapore, 2020, pp. 95–126.
41. Battistoni M, Som S and Powell CF. Highly resolved Eulerian simulations of fuel spray transients in single and multi-hole injectors: Nozzle flow and near-exit dynamics. *Fuel* 2019; 251(4): 709–729.
42. Zhang Y, Qi B, Guo D and Guo Y. Optimization of injector nozzle in high pressure common rail injection system. *J Mech Eng Res Dev* 2018; 41(1): 27–37.
43. Lee JH, Cho S, Lee SY and Bae C. Bouncing of the diesel injector needle at the closing stage. *Proc Inst Mech Eng Part D J Automob Eng* 2002; 216(8): 691–700.
44. Yasutomi K, Hwang J, Manin J, Pickett L, Arenti M, Daly S and Skeen S. Diesel injector elasticity effects on internal nozzle flow. SAE Technical Paper 2019-01-2279, 2019.
45. Gibson DH, Dionne PJ and Singhal AK. A numerical model for elastohydrodynamic analysis of plunger and barrel clearances in fuel injection equipment. *J Tribol* 1994; 116(3): 597–605.
46. Marčić S, Marčić M and Praunseis Z. Mathematical model for the injector of a common rail fuel-injection system. *Engineering* 2015; 7(6): 307–321.
47. Qi B, Zhang Y and Guo D. Study on seal performance of injector nozzle in high-pressure common rail injection system. *J Brazilian Soc Mech Sci Eng* 2018; 40(2): 97.
48. Lazarev VE, Wloka JA and Wachtmeister G. A method for the estimation of the service life of a precision guiding interface ‘needle-nozzle body’ of a common-rail-injector for high rail pressures. SAE technical paper 2011-01-2020, 2011.
49. Wu D, Sun B and Xu D. Deformation of nozzle, needle, and control plunger of solenoid fuel injector under high injection pressure. *Proc Inst Mech Eng Part D J Automob Eng* 2019; 233(7): 1767–1782.
50. Xu D, Sun B, Yang Q and Wu D. Investigation on the deformation of injector components and its influence on the injection process. SAE Technical Paper 2020-01-1398, 2020.
51. Dongiovanni C and Coppo M. Accurate modelling of an injector for common rail systems. *Fuel Inject* 2010; 95–120.
52. Ferrari A and Mittica A. FEM modeling of the piezoelectric driving system in the design of direct-acting diesel injectors. *Appl. Energy* 2012; 99: 471–483.
53. Coppo M and Dongiovanni C. Experimental validation of a common-rail injector model in the whole operation field. *J Eng Gas Turbines Power* 2007; 129(2): 596.
54. Chiavola O and Palmieri F. Modeling needle motion influence on nozzle flow in high pressure injection system. SAE technical paper 2007-01-0250, 2007.
55. Salvador FJ, Martinez J, Romero V and Rosello D. Study of the influence of the needle eccentricity on the internal flow in diesel injector nozzles by CFD calculations. *Int J Com Mathe* 2014; 91: 24–31.
56. Chiavola O and Palmieri F. On a modified VCO nozzle layout for diesel common rail injectors under actual needle displacement. *Energy Procedia* 2017; 126: 1027–1034.
57. Greif D, Sampl P and Edelbauer W. Cavitating injector flow simulations considering longitudinal and lateral needle displacement. *Int J Automob Eng* 2014; 5(4): 85–90.
58. Xue Q, Som S, Battistoni M, Longman DE, Zhao H, Senecal P and Pomraning E. Three-dimensional simulations of the transient internal flow in a diesel injector: effects of needle movement. In: *Proceedings of the ILASS Americas, 25th Annual Conference on Liquid Atomization and Spray Systems*, Pittsburgh, USA, May 2013, pp. 1–13.
59. Gibson RF. *Principles of Composite Material Mechanics*. 2016. Florida, USA, CRC press.
60. Toupin RA. Saint-Venant’s Principle. *Arch Ration Mech Anal* 1965; 18: 83–96.
61. Luo T, Jiang S, Moro A, Wang C, Zhou L and Luo F. Measurement and validation of hole-to-hole fuel injection rate from a diesel injector. *Flow Meas Instrum* 2018; 61: 66–78.
62. Luo F, Jiang S, Moro A, Luo T, Zhou L and Wu X. The development of a data acquisition system for measuring the injection rate of a multihole diesel injector. *Sensors Actuators, A Phys* 2017; 261: 166–176.

63. Maiti DK and Bhatt R. Interactions of vortices of a square cylinder and a rectangular vortex generator under Couette-Poiseuille flow. *J. Fluids Eng Trans ASME* 2015; 137(5): 051203.
64. Qian D and Liao R. Theoretical analysis and mathematical modelling of a high-pressure pump in the common rail injection system for diesel engines. *Proc Inst Mech Eng Part A J Power Energy* 2015; 229(1): 60–72.

Notation

Symbol

$d (m)$	the diameter
$l (m)$	the length
$e (m)$	the lateral displacement

α	dip angle between the axis of the needle and needle body (after eccentricity and deformation)
$F (N)$	resultant force of the spring force and control plunger applied force
$P (Pa)$	Fuel pressure
$f (Pa)$	stress acts on the inlet and outlet of the clearance
$m (g)$	mass
$M (N \cdot m)$	bending momentum
$E (Pa)$	elastic modulus
$I (m^4)$	inertia moment
$\delta (m)$	lateral displacement of the needle/needle body
λ	Poisson ratio